Int J Earth Sci (Geol Rundsch) (2006) 95: 2–18
DOI 10.1007/s00531-005-0011-4

ORIGINAL PAPER

Caroline Sassier · Philippe Boulvais · Denis Gapais
Ramon Capdevila · Hervé Diot

From granitoid to kyanite-bearing micaschist during fluid-assisted shearing (Ile d'Yeu, France)

Received: 24 September 2004 / Accepted: 26 May 2005 / Published online: 26 July 2005

Abstract We describe amphibolite-facies shear zones affecting an orthogneiss from the Armorican Hercynian belt (Ile d'Yeu, western France). The deformation pattern is consistent with top-to-the-South thrusting followed by E–W extension, as documented elsewhere in the region. Shearing was accompanied by channelled fluid flow that transformed the orthogneiss into a peraluminous micaschist. Structural and mineralogical data indicate rather early strain localization. Then, temperature increase associated with crustal thickening favoured more distributed deformations marked by shear zone stretching and the development of a HT regional foliation. Chemical analyses made across five shear zones show mass transfers that mainly implied losses in Ca and Na, and gains in H_2O, Mg, and K. Most results indicate constant volume transformation, but some suggest records of either gains or losses of volume (between +20% and −30%). This might reflect variable records of fluid-rock interactions according to the timing of initiation and subsequent evolution of individual shear zones, early thrusting stages being marked by up-temperature flow, and late thrusting stages by down-temperature flow. $\delta^{18}O$ analyses suggest that fluids experienced significant isotopic exchange with orthogneisses.

Keywords Shear zones · Mass transfers · Fluid-rock interactions · High-temperature deformation · ranitic rocks

C. Sassier · P. Boulvais · D. Gapais · R. Capdevila
Géosciences Rennes, UMR 6118 CNRS,
Université de Rennes 1, Rennes cedex, 35042, France

H. Diot
Pôle Sciences et Technologie, Université de La Rochelle,
Av. Michel Crepeau, La Rochelle Cedex 01, 17042, France

Present address: C. Sassier
Laboratoire de Sciences de la Terre, UMR 5570 CNRS,
Université de Lyon 1, Villeurbanne cedex, 69622, France
E-mail: caroline.sassier@univ-lyon1.fr

Introduction

Interactions between strain localization, fluid circulation and chemical mass transfers across shear zones have been extensively studied in the past 30 years (see Beach 1976; Etheridge et al. 1983, 1984; Kerrich 1986; McCaig 1988; Yonkee et al. 2003). Many works have in particular documented softening processes associated with metamorphic reactions and fluid channelling in the granitic crust (e.g. Mitra 1978; White and Knipe 1978; Marquer et al. 1985; Marquer and Burkhard 1992; Fitzgerald and Stünitz 1993; Wibberley 1999). Most examples concern the upper crust, where strain localization is common. On the other hand, only few examples have reported strong interactions between shearing, mass transfers and metamorphic reactions within hot and deep parts of the crust (Dipple et al. 1990; Selverstone et al. 1991; Cartwright and Buick 1999). Indeed, most efficient reaction softening processes, like feldspar-to-mica decay, involve important water input; whereas the environment of a stable lower crust is generally water deficient (Newton 1990). In addition, increasing temperature generally promotes distributed deformations of granitic rocks because of overall decrease in strength contrast between feldspars and quartz (see Gapais 1989).

The present paper describes an orthogneiss from the Ile d'Yeu (south Brittany, France) located in the internal zones of the Armorican Hercynian belt. During the Hercynian collision, the region underwent crustal thickening, followed by syn-convergence extension in Upper Carboniferous times (see Gapais et al. 1993; Burg et al. 1994; Cagnard et al. 2004). The Ile d'Yeu orthogneiss is thrust over metasediments. It is affected by a penetrative flat-lying fabric associated with amphibolite facies metamorphism (Semelin and Marchand 1984), and is locally affected by strong strain localization within metre-scale ductile shear zones. Shear zones show drastic changes in modal composition, from primary weakly peraluminous magmatic assemblages (Qtz + Kfs + Pl + Bt) to strongly peralumi-

nous ones (Qtz + Bt + Ms ± Ky). A combined analysis of structures, microstructures, petrology and geochemistry across several shear zones attests to important fluid-assisted mass transfers during shearing. The study leads to an integrated model of the formation and evolution of the shear zones during the tectonic history of the Ile d'Yeu, from thrusting to subsequent exhumation.

Tectonic setting

The southern part of the Armorican Hercynian belt (Fig. 1) is bounded to the North by the South Armorican Shear Zone, a major dextral wrench zone (Jégouzo 1980). It shows three main groups of tectonic units (Fig. 1). Uppermost ones are marked by metamorphic histories of HP-LT type, with blueschists (Bois de Céné and Ile de Groix blueschists, 1,400–1,900 MPa, 500–550°C; Bosse et al. 2002 and references therein) overlying metamorphic volcanics and shales (Vendée and Belle-Ile-en-Mer porphyroids, 700–900 MPa, 350–400°C; Le Hébel et al. 2002). Burial and exhumation of these units occurred during Upper Devonian to Lower Carboniferous times (370–350 Ma, Bosse et al. 2002; Le Hébel et al. 2002). HP-LT units are underlain by metasediments affected by a Barrovian metamorphism increasing downward from anchizonal facies to amphibolite facies conditions (Triboulet and Audren 1988; Goujou 1992 and references therein). The bottom of the pile consists of high temperature rocks with large volumes of migmatites where local estimates of peak metamorphic conditions yielded values of the order of 700–750°C and 800–1,000 MPa (Jones and Brown 1990; Goujou 1992). Associated geochronological data (Ar-Ar on amphiboles and micas, U-Pb on monazites) indicate rapid cooling of the lower units during the Upper Carboniferous, around 310–300 Ma (see Goujou 1992; Gapais et al. 1993; Brown and Dallmeyer 1996). Recent works have shown that exhumation was associated with regional-scale extension (Gapais et al. 1993; Cagnard et al. 2004). The resulting overall pattern is that of exhumed windows cored by HT rocks and surrounded by klippen of HP-LT units showing records of earlier thrusting (Fig. 1).

The Ile d'Yeu orthogneiss belongs to the lowermost part of the tectonic pile exposed in South Brittany. Its equivalent on the continent is found in the Sables

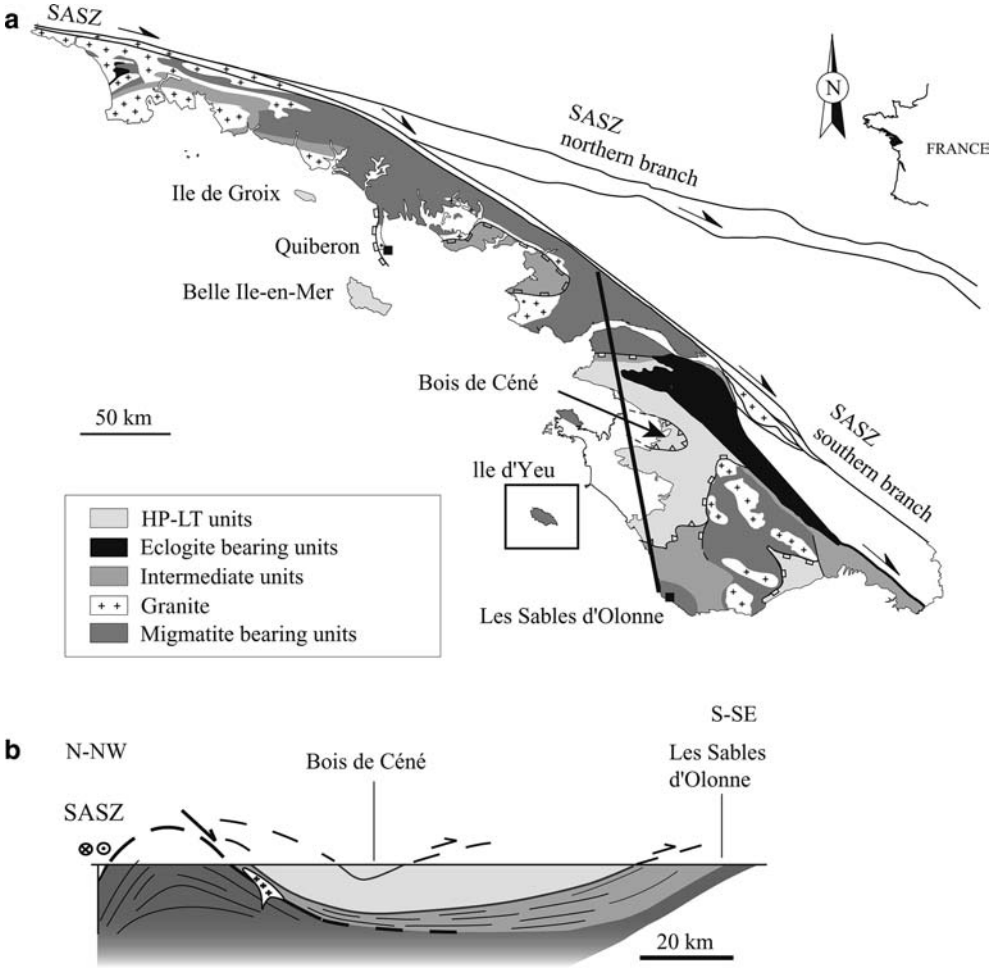

Fig. 1 Location of the Ile d'Yeu within the Hercynian belt of South Brittany (modified after Cagnard et al. 2004). **a** Simplified tectonic and metamorphic map. **b** General cross-section. The Ile d'Yeu orthogneiss belongs to the lowermost migmatite-bearing units that crop-out in the region

d'Olonne area (Fig. 1; Mathieu 1945). There, main deformations occurred under partial melting conditions and are associated with southward thrusting (Iglesias and Brun 1976; Brun and Burg 1982; Cannat and Bouchez 1986) overprinted by E–W extension-induced crustal thinning (Colchen and Rolin 2001; Cagnard et al. 2004). If extensional deformations are well bracketed around 310–300 Ma, the age of the thrusting event remains unknown.

The Ile d'Yeu orthogneiss comprises sheets of various compositions, including granodiorite, syenogranite and porphyric granite (Diot et al. 2002) (Fig. 2). Orthogneisses are thrust over paragneisses that mainly crop out in a window in the southern part of the island (Fig. 2). There, Semelin and Marchand (1984) have studied peraluminous rocks made of alternating biotitites and kyanite-bearing gneisses. They recognized three main successive events in the metamorphic evolution: (1) St + Ky + Grt + Bt + Ms assemblages indicating Barrovian metamorphic conditions, with temperatures around 600°C and minimum pressures of the order of 500 MPa, (2) the occurrence of sillimanite and associations of cordierite-corindon and cordierite-spinel indicating anatectic conditions, and (3) growth of andalusite, sericite and chlorite during limited retrogression. This metamorphic history is consistent with that recorded in the Sables d'Olonne area (Goujou 1992; Cagnard et al. 2004).

Outcrop-scale structures

Regional foliation and lineation

Most outcrops of the Ile d'Yeu consist of well-foliated orthogneiss. Fabrics reflecting either moderate or very large deformations occur locally (Fig. 3a, b). The foliation strikes E–W on the north coast to NE on the west and south coast, with an overall northward dip of about 10° (Fig. 4). It bears a well developed stretching linea-

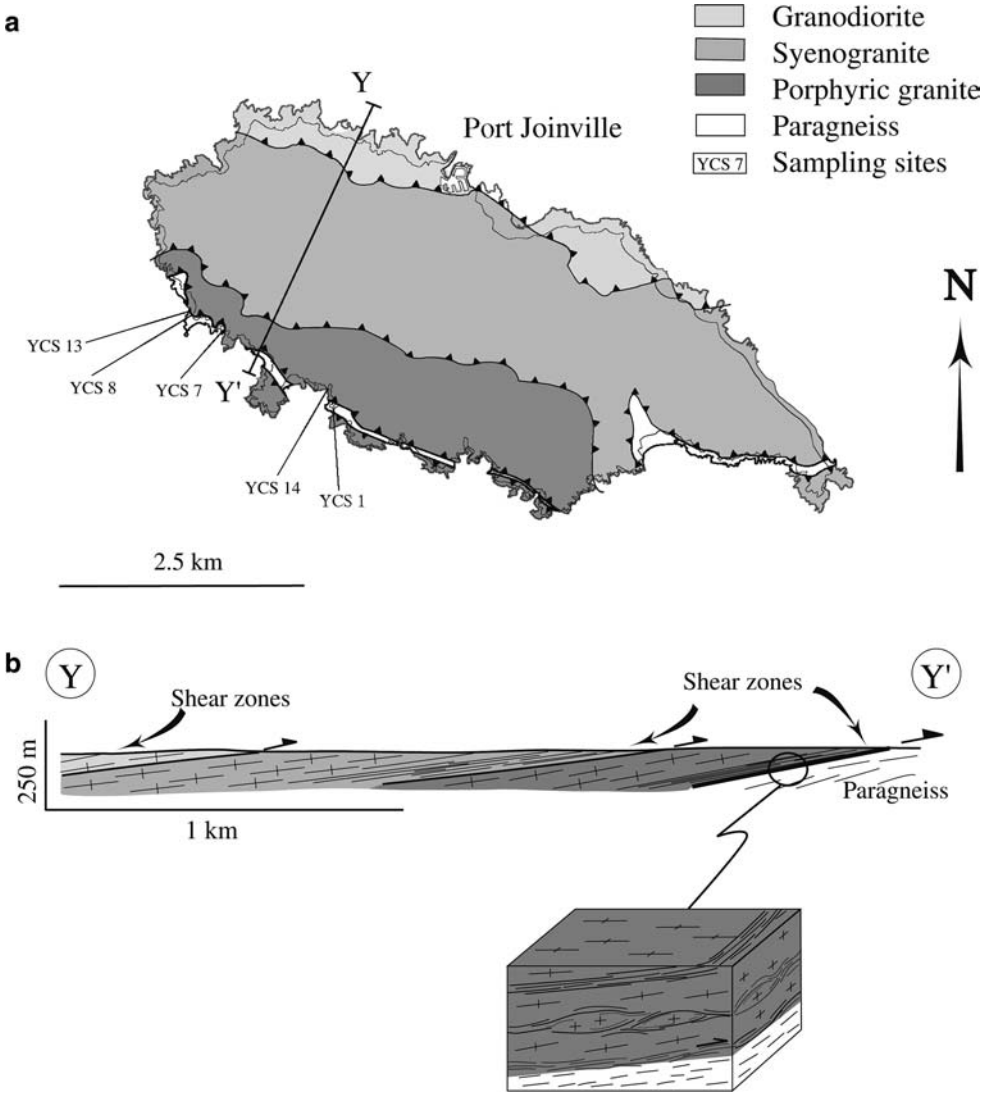

Fig. 2 Simplified geological map (**a**) and cross-section (**b**) of the Ile d'Yeu area (modified after Diot et al. 2002), and sampling localities

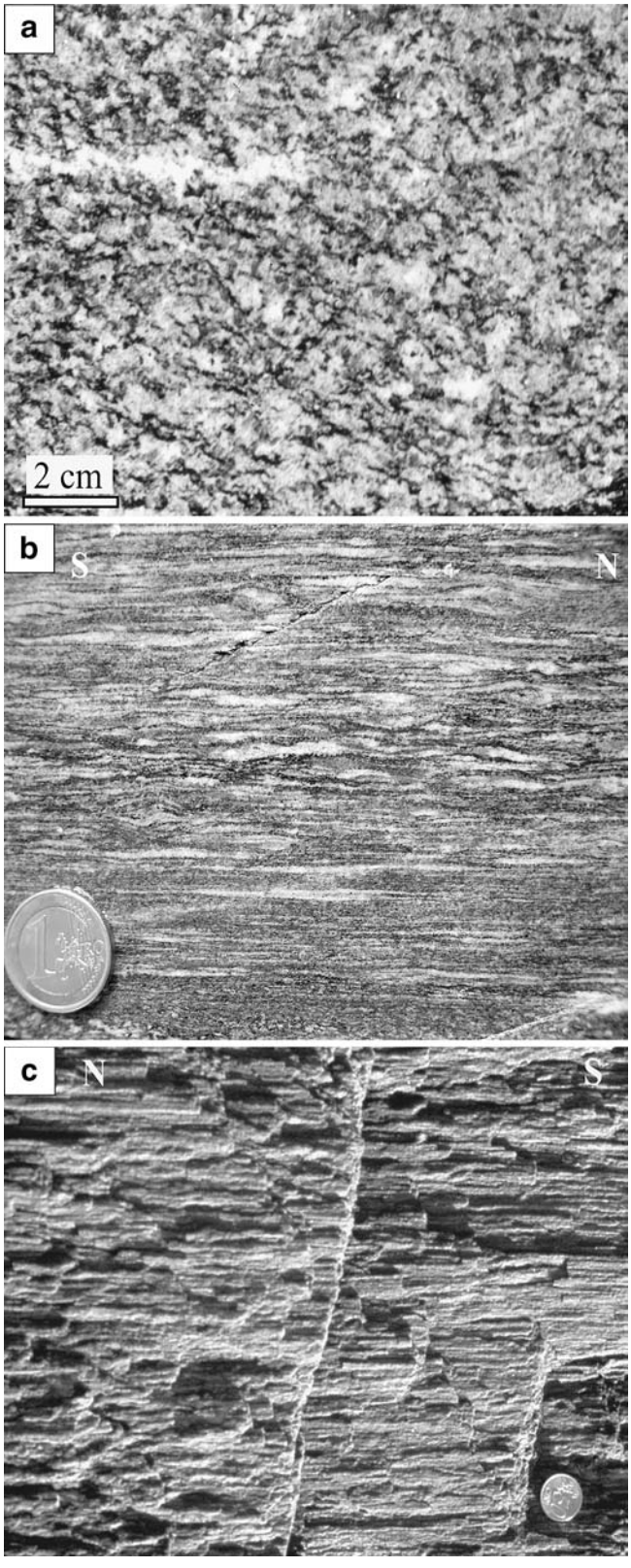

Fig. 3 Photographs showing moderately (**a**) and strongly (**b**) deformed orthogneiss (views perpendicular to foliation and parallel to stretching lineation), and regional stretching lineation (**c**) (view parallel to the sub-horizontal foliation)

tion (Fig. 3c) that strikes dominantly N to NW along the northern coast of the island and around NW on the other coastal outcrops (Fig. 4). Kinematic indicators, especially shear bands, attest to overall top-to-the-South thrusting (Diot et al. 2002).

Shear zones

The regional foliation is locally associated with an array of metre-scale mylonitic shear zones anastomosed around flat lenses of orthogneiss (Fig. 5a–c). In the field, shear zones appear as dark bands (Fig. 5a–c) due to a decrease in grain size and to mineralogical changes especially marked by an increase in biotite content.

Most shear zones are flat lying, at very low angle to the orthogneiss foliation (Fig. 5a–c). Where they wrap around decimetre to metre-thick lenses of orthogneiss, the latter often show boudinage, with biotite-rich mylonitic material filing boudin necks (Fig. 5d). These features show that most shear zones underwent parallel stretch and reorientation during regional deformation. Only few shear zones are significantly oblique to the orthogneiss foliation (Fig. 5c).

Within shear zones, the attitude of foliation and stretching lineation is consistent with the fabric of the surrounding orthogneiss (Fig. 4). The main difference is an important scatter of lineation strikes in some areas, between dominantly NS to NW and E–W (Fig. 4). Boudins (Fig. 5d), as well as lineation patterns, indicate local E–W to NW–SE stretching. The scatter of principal stretch directions between E–W and N–S can be locally observed at outcrop-scale and suggests regional finite strains of flattening type.

Shear zones, especially those lying at low angle to the regional foliation, are marked by very sharp strain gradients (Fig. 6a). Across shear zones oblique to the regional foliation, changes from orthogneiss to mylonite are also sharp, but may be more gradual (Fig. 6b).

Microstructures and mineralogy

Our study mainly focused on the southern part of the Ile d'Yeu, where the orthogneiss consists of Qtz + Plg + Kfs + Bt ± Ms. Garnet-bearing orthogneiss is locally observed.

Five groups of samples selected across five individual shear zones have been analysed (Fig. 2). Four of them (YCS 1, 8, 13, 14) are from low-angle shear zones with sharp strain gradients. One (YCS 7) is from an oblique shear zone (Figs. 5c, 6b). For each zone, we sampled the mylonite and the adjacent less deformed orthogneiss (sampled at less than one metre away from the shear zone). Where strain gradients were not too sharp, intermediate stages were also sampled.

The general texture of the orthogneiss is granoblastic. Both K-feldspar and plagioclase show syn-kinematic

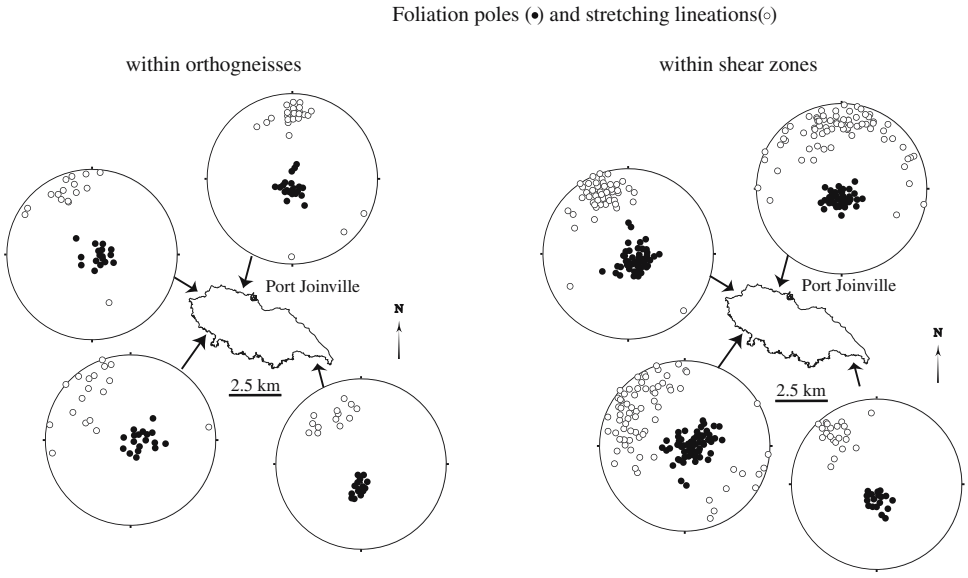

Fig. 4 Poles to foliation (*black circles*) and stretching lineations (*open circles*) within orthogneisses and shear zones along the different coasts of the Ile d'Yeu (equal angle, lower hemisphere projections)

recrystallisation (Fig. 7a, b), which indicates amphibolite-facies conditions (Voll 1976; Simpson 1985; Gapais 1989). Furthermore, large recrystallized feldspar grains are riddled with numerous inclusions of quartz (Fig. 7b), a feature typical of subsolidus or partial melting HT environments (Ashworth 1986; Gapais et al. 1987). Quartz grains have lobate boundaries, attesting to extensive grain boundary migration. They also display subgrain boundaries defining chessboard textures (see Blenkinsop 2000) (Fig. 7c). These indicate combined intracrystalline slip along <a> and <c> directions, a feature that attests to HT sub-solidus plasticity (Gapais and Barbarin 1986; Mainprice et al. 1986).

Strain gradients across shear zones are marked by a strong grain size reduction, an important decrease in feldspar content, and an increase in biotite and muscovite contents (Fig. 7d). Enrichment in apatite content is also observed locally. Quartz may occur as ribbons and has often a chessboard texture. Mylonites can be strongly peraluminous, with Bt + Ms + Qtz + Ky assemblages (sample YCS 13e) (Fig. 7e). In these rocks, syn-kinematic kyanite crystals are elongate within the foliation and are generally bounded by retrogressive undeformed cordierite rims (Fig. 7e).

Microprobe analyses of minerals made across some shear zones (Table 1) underline changes in mineral compositions with increasing strain. These are marked by (1) an increase in Mg and Al contents within biotites in mylonites (Fig. 8a), (2) an increase in Mg and Na contents within muscovites (Fig. 8b), and (3) an increase in Mg and Cl contents within apatites (Fig. 8c). The scatter of biotite compositions within orthogneisses (Fig. 8a) is too large to be explained by Ti vacancies at high temperature, and may rather reflect the existence of two biotite generations. Apatites from the high-angle shear zone (series YCS 7) tend to show a lower increase in Mg and Cl than those from the low-angle ones (Fig. 8c).

Whole-rock geochemistry

Among the orthogneisses, four have compositions compatible with igneous rocks in the Hughes's (1973) diagram (Fig. 9a). These are three granodiorites (YCS 1a, 7a, 8a) and one granite (YCS 14a) that show slightly peraluminous compositions (Fig. 9b; Maniar and Piccoli 1989) and may be considered as close to magmatic protoliths. All display the same calc-alkaline patterns with high Th/LREE and LREE/Zr ratios and large Ta and Nb negative anomalies (Fig. 10a). REE patterns are also typical of calc-alkaline rocks (LREE enriched, and low fractionation of HREE, with $(La/Yb)_N$ between 2.9 and 7.3) (Fig. 10b).

In contrast, all other samples, that include mylonites and one moderately deformed sample (YCS 13a), are too rich in K and too peraluminous compared with igneous rocks (Fig. 9a, b). However, the overall patterns of Fig. 10 show that both orthogneisses and mylonites (including the kyanite-bearing one YCS 13e) are derived from a similar igneous protolith. The age of the protolith is not precisely established. Pilot U-Pb analyses have suggested an age around 600 Ma (Wyns et al. 1986), and new dating is presently in progress.

Mass transfers across shear zones

Chemical compositions of shear zones lie outside the field of igneous rocks (Fig. 9a) and have a strong peraluminous signature related to hydration (Fig. 9b), which emphasizes their metasomatic nature. Within shear zones, the LOI (mainly water content) is increased up to 4.5 wt%. In Fig. 11, variations of MgO, CaO and Na_2O with LOI argue for the mobility of these elements, namely input of MgO (as well as K_2O, Fig. 9a) and leaching of CaO and Na_2O.

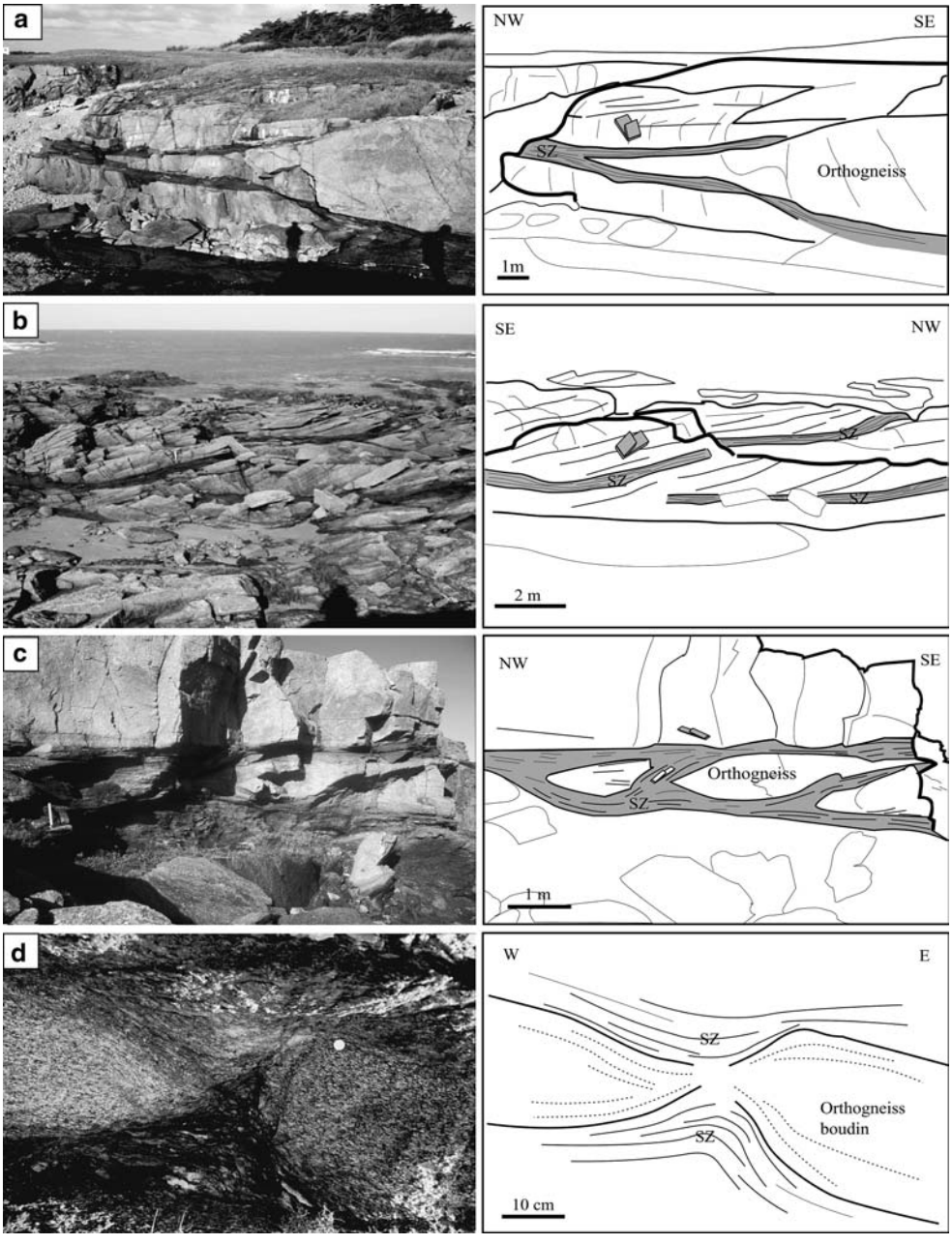

Fig. 5 Outcrop-scale aspects of shear zone arrays. Shear zones (SZ) are mainly flat lying at very low angle to regional foliation (**a** and **b**, southern and northern coast, respectively), and locally oblique to the foliation (**c**). *Arrows* show apparent shear senses. **d** Example of E–W boudinage of orthogneiss lenses between two biotite-rich shear zones

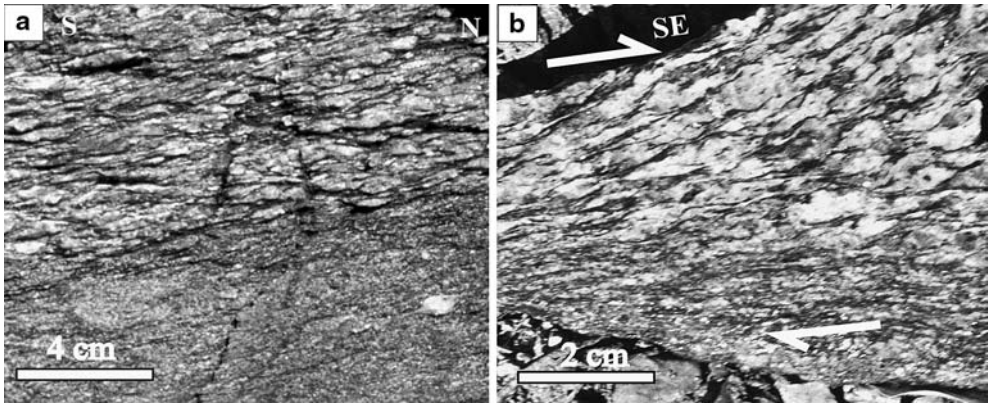

Fig. 6 Aspects of strain gradients across shear zones (views perpendicular to foliation and parallel to stretching lineation). **a** Outcrop showing a very sharp gradient across a flat-lying shear zone. **b** Sawed section of sample showing a more gradual strain increase across an oblique shear zone (series 7)

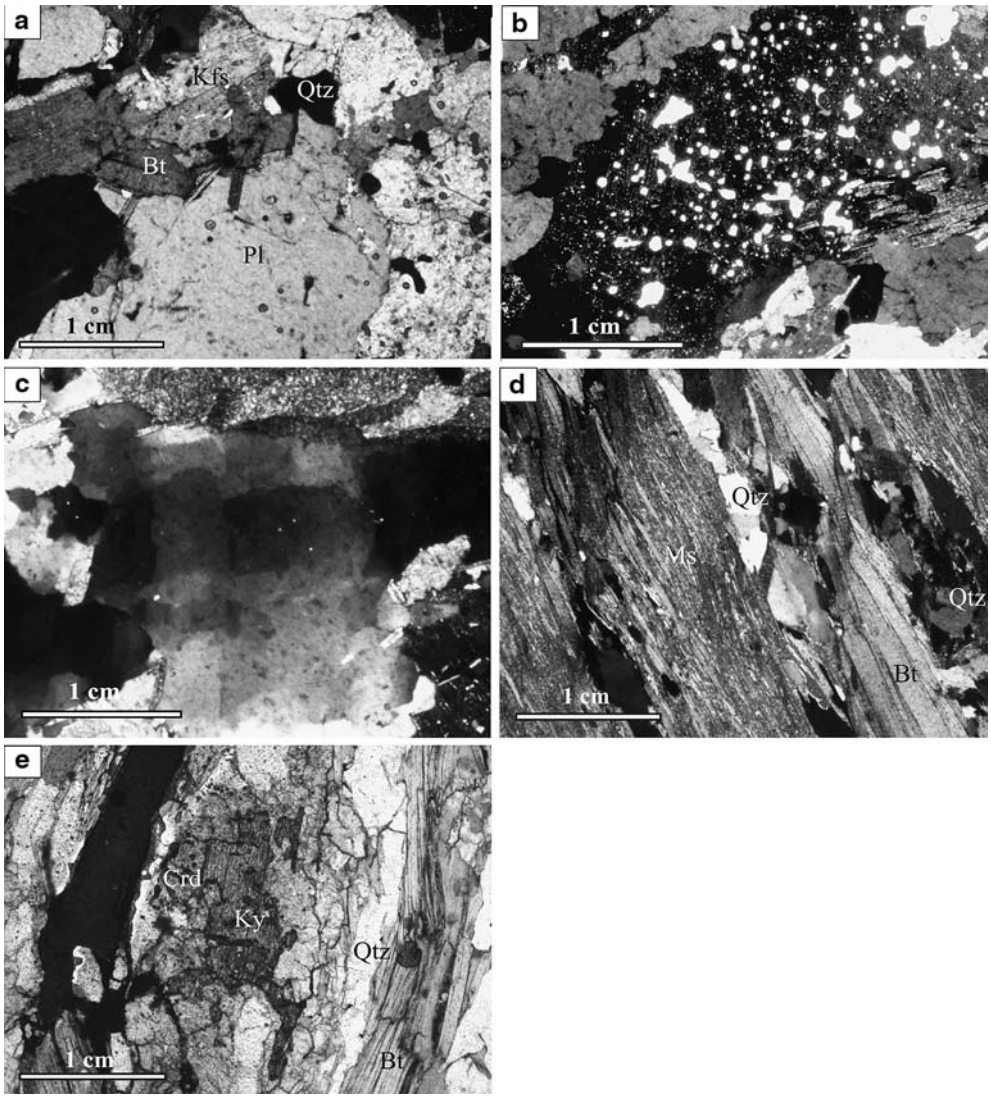

Fig. 7 Deformation microstructures. **a** General orthogneiss microstructure. **b** Typical aspect of large recrystallized feldspars riddled with quartz inclusions. **c** Chessboard subgrain structure within a quartz grain. **d** Mica-enriched and feldspar-depleted mylonite within shear zone. **e** Mylonite showing oriented syn-kinematic kyanite crystal partly retrogressed to cordierite. *Bt* biotite; *Crd* cordierite; *Kfs* K-feldspar; *Ky* kyanite; *Ms* muscovite; *Pl* plagioclase; *Qtz* quartz

Further quantification of mass transfers across individual shear zones has been attempted using the Grant's isocon technique (Fig. 12). Isocon analysis requires (1) to make a reliable estimate of the composition of the protolith, and (2) to identify immobile elements that may define a reliable isocon.

Protolith estimates

The high SiO_2 content (76.5%, Table 2) and the low Zr content (115 ppm, Table 2) of sample YCS 14a show that this rock underwent substantial magmatic differentiation. As sample 14b does not show such depletion in Zr (Zr = 262 ppm), it may derive from a less differentiated protolith than sample 14a. In order to estimate chemical changes within sample 14b, we therefore chose to use a mean protolith calculated from the three less differentiated protoliths (YCS 1, 7a, and 8a). This allowed us to draw a reasonably well-defined isocon (Fig. 12a), which was actually not the case using sample 14a. For series 13, as sample 13a does not correspond to an unaltered protolith (Fig. 9a), we have used the mean protolith defined above to identify the chemical changes in this sample (Fig. 12b). Chemical changes between samples 13e and 13c are then considered relative to the less deformed sample 13a. This provides minimum estimates of element mobility for these two samples (Fig. 12c, d). For the three other shear zones (1, 8 and 7) (Fig. 12e–h), no major structural or chemical arguments indicate that the less deformed sample of each series might differ from the real protolith.

Identification of immobile elements

For granitic rocks, isocons are classically drawn using elements such as Al (+Ga), Ti, P, Zr, Hf, Nb, Ta, and REE, which are generally immobile. Some of these elements show unusual behaviour in the Ile d'Yeu shear zones. For example, the ratio Ga/Al is increased in several mylonites (e.g. 10,000*Ga/Al of 3.0 for sample

Table 1 Mean chemical compositions of biotite, apatite and muscovite across three selected shear zones (sampling sites 7, 8 and 13) (Camebax SX 50 microprobe, Brest). Operation conditions were 15 kV, sample current of 20 nA, and counting time for each analysis was 15 s

	Biotite		Muscovite		Apatite	
	Orthogneiss ($N=48$)	Shear zone ($N=64$)	Orthogneiss ($N=25$)	Shear zone ($N=49$)	Orthogneiss ($N=11$)	Shear zone ($N=10$)
Wt% oxide						
SiO_2	35.50 ± 0.65	37.02 ± 0.75	45.99 ± 0.44	45.76 ± 1.09	0.16 ± 0.13	0.05 ± 0.08
TiO_2	3.43 ± 0.51	1.72 ± 0.32	1.47 ± 0.73	0.54 ± 0.30	0.02 ± 0.03	0.02 ± 0.03
Al_2O_3	17.93 ± 1.30	19.73 ± 0.91	34.69 ± 0.92	35.60 ± 1.57	0.03 ± 0.06	0.19 ± 0.41
Cr_2O_3	0.03 ± 0.04	0.03 ± 0.04	0.08 ± 0.30	0.02 ± 0.03	0.01 ± 0.03	0.01 ± 0.02
FeO*	20.29 ± 1.66	12.17 ± 0.78	1.27 ± 0.15	0.85 ± 0.21	0.26 ± 0.12	0.19 ± 0.05
MnO	0.17 ± 0.07	0.08 ± 0.07	0.02 ± 0.03	0.02 ± 0.04	0.15 ± 0.10	0.18 ± 0.10
MgO	8.72 ± 0.51	14.19 ± 0.84	0.67 ± 0.15	0.93 ± 0.34	0.02 ± 0.04	0.06 ± 0.03
CaO	0.00	0.02 ± 0.04	0.00	0.01 ± 0.01	55.54 ± 0.61	54.81 ± 0.62
Na_2O	0.14 ± 0.04	0.26 ± 0.08	0.49 ± 0.11	0.68 ± 0.18	0.06 ± 0.03	0.07 ± 0.02
K_2O	9.92 ± 0.38	9.71 ± 0.43	10.92 ± 0.20	10.52 ± 0.68	0.05 ± 0.07	0.02 ± 0.05
P_2O_5	0.00	0.00	0.00	0.00	43.67 ± 0.41	43.63 ± 0.40
Cl	0.04 ± 0.03	0.02 ± 0.02	0.01 ± 0.01	0.01 ± 0.01	0.05 ± 0.04	0.20 ± 0.08
F	0.01 ± 0.01	0.01 ± 0.01	0.01 ± 0.01	0.01 ± 0.01	3.42 ± 0.11	3.37 ± 0.08
Total	96.19 ± 0.61	94.96 ± 0.95	95.62 ± 0.85	94.97 ± 0.63	103.46 ± 0.66	102.81 ± 0.77
Formula	*22O*	*22O*	*22O*	*22O*		
Si	5.41 ± 0.07	5.45 ± 0.07	6.13 ± 0.05	6.11 ± 0.14		
Ti	0.39 ± 0.06	0.19 ± 0.04	0.15 ± 0.07	0.05 ± 0.03		
Al	3.22 ± 0.21	3.42 ± 0.15	5.45 ± 0.14	5.60 ± 0.24		
Cr	0.00	0.00	0.01 ± 0.03	0.00		
Fe	2.59 ± o.24	1.50 ± 0.11	0.14 ± 0.02	0.10 ± 0.02		
Mn	0.02 ± 0.01	0.01 ± 0.01	0.00	0.00		
Mg	1.98 ± 0.10	3.11 ± 0.17	0.13 ± 0.03	0.19 ± 0.07		
Ca	0.00	0.00	0.00	0.00		
Na	0.04 ± 0.01	0.07 ± 0.02	0.13 ± 0.03	0.18 ± 0.05		
K	1.93 ± 0.07	1.82 ± 0.08	1.86 ± 0.03	1.79 ± 0.12		
P	0.00	0.00	0.00	0.00		
Cl	0.00	0.00	0.00	0.00		
F	0.00	0.00	0.00	0.00		
Total	15.58 ± 0.07	15.59 ± 0.05	13.99 ± 0.04	14.02 ± 0.08		
XCL					0.008 ± 0.006	0.031 ± 0.013
XMg	0.43 ± 0.03	0.67 ± 0.03	0.48 ± 0.06	0.65 ± 0.06		

XMg molar Mg/(Mg + Fe); *XCl* molar Cl/(Cl + F)

8c, and up to 4.6 in sample YCS 1b) with respect to orthogneisses (10,000*Ga/Al close to a classical value of 2.6 for most granitic rocks). Because this might possibly reflect Al and (or) Ga mobility, these elements were excluded for isocon estimates. REE also display some erratic behaviour with respect to other LIL elements such as Zr or Th, and have therefore also been excluded for isocon estimates. Consistently, REE lie generally significantly away from the isocon lines (Fig. 12). Moreover, the mylonite 7c shows a decrease in REE content with respect to the protolith 7a, whereas the intermediate deformation stage 7b shows an increase (Fig. 12g, h). Such a peculiar behaviour has recently been described in Alpine shear zones by Rolland et al. (2003) who explained these small-scale variations as the result of local redistribution through a fluid phase by alteration of pre-existing magmatic REE-bearing minerals and precipitation of syn-tectonic REE-bearing others. With respect to the protolith YCS 1a, sample YCS 1b is marked by (1) an important apatite precipitation with input of P_2O_5 ($P_2O_5 = 0.88\%$, Table 2), (2) a much higher Nb/Ta ratio and (3) a depletion in Th and U (Table 2). For these reasons, all these elements have not been considered for the isocon estimate (Fig. 12e).

Element mobility

Figure 12 underlines that most shear zones show a significant increase in amounts of K, Rb, Mg, and LOI (mainly H_2O), and a decrease in Ca, Na, Pb and Sr (Fig. 12a, e, f–h). Losses in Ca, Sr and Na can be attributed to the disappearance of plagioclase. The important amount of biotite and the growth of muscovite within shear zones are consistent with the increase in Mg, K, Rb and H_2O contents. Significant gains in W and Sn are also observed within many mylonites (Fig. 12a, e–h).

Series 13 displays a peculiar behaviour. Indeed, K and Mg are gained in sample 13a relative to the mean protolith (Fig. 12b), but are lost between sample 13a and the kyanite-bearing sample 13e (Fig. 12e). Figure 12c underlines that sample 13a is modified with respect to the shear zone protholith, this sample showing an element distribution identical to that of the substantially

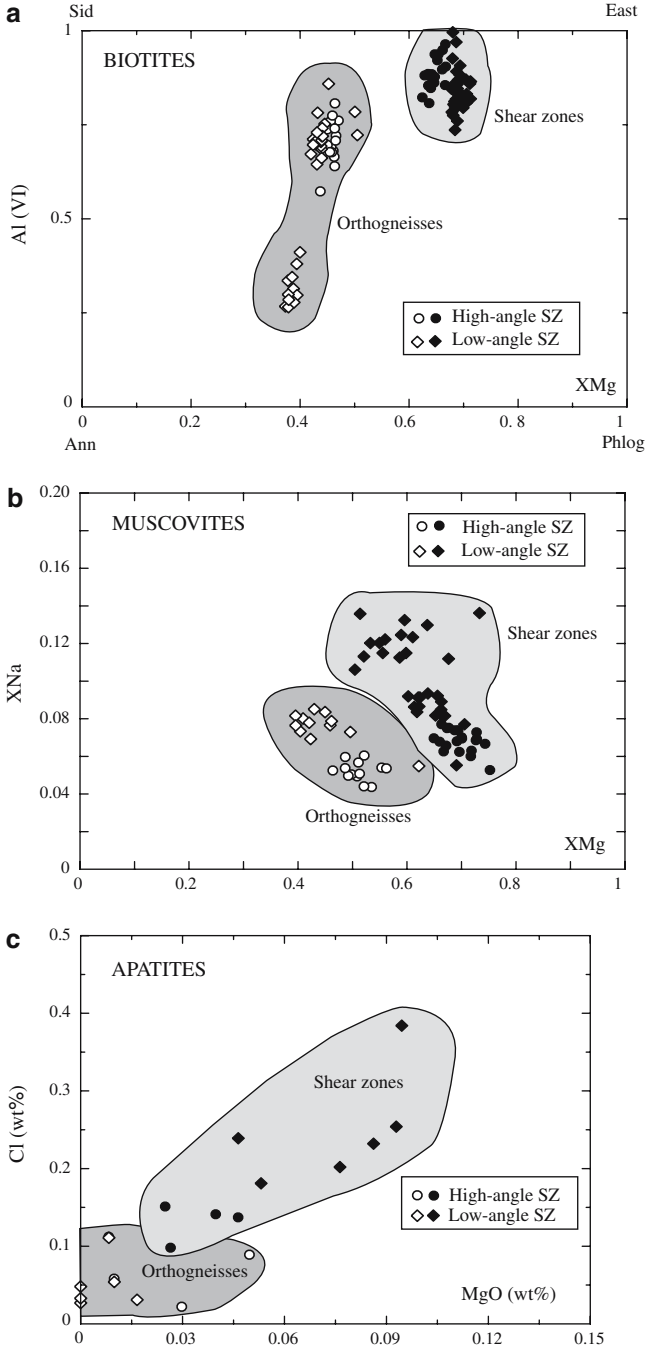

Fig. 8 Changes in mineral compositions between orthogneisses and shear zones (see Table 1). **a** Al (VI) versus XMg (Mg/Mg + Fe) diagram showing biotite compositions between annite (*Ann*), siderophyllite (*Sid*), eastonite (*East*) and phlogopite (*Phl*) end members. **b** XNa (= Na/(Na + K)) versus XMg (= Mg/(Mg + Fe)) ratios in muscovite. **c** Chlorine (Cl) versus MgO contents (wt%) in apatite

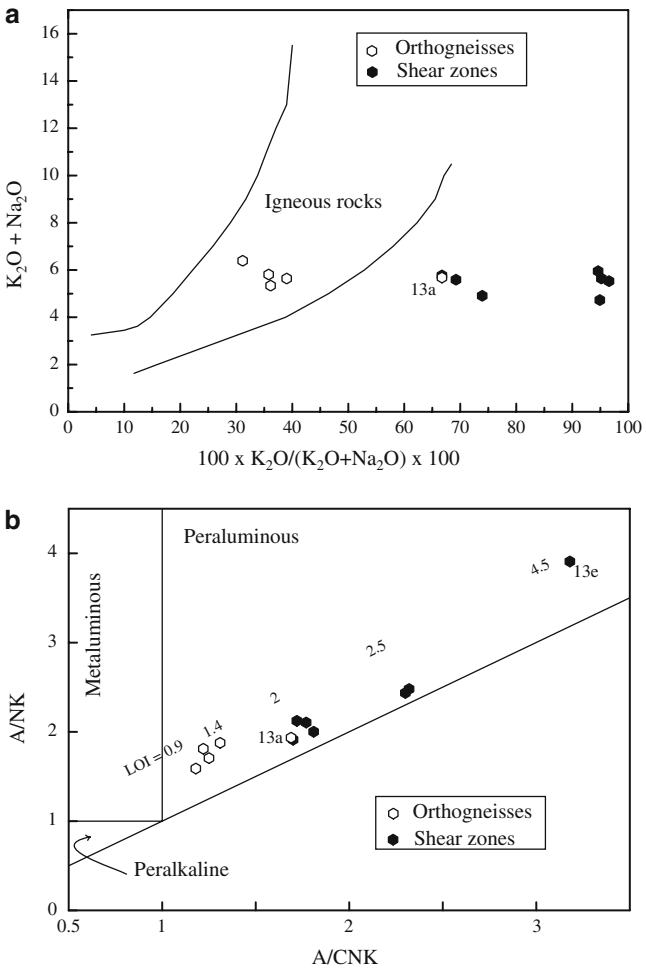

Fig. 9 **a** Whole-rock composition in a ($Na_2O + K_2O$) versus K_2O/($K_2O + Na_2O$) (wt%) diagram (Hughes 1973). Shear zone rocks are enriched in K_2O compared with less deformed orthogneisses. The sum of alkaline oxydes is rather stable, which reflects replacement of Na by K within the rock. 13a is the less deformed sample of series YCS 13. **b** Whole-rock composition in an A/NK (Al_2O_3/($Na_2O + K_2O$)) versus A/CNK (Al_2O_3/($CaO + Na_2O + K_2O$)) diagram (molecular proportions) (Maniar and Piccoli 1989). Loss on ignition (*LOI*) is indicated by numbers. Deformed rocks are strongly peraluminous, mainly because of hydration that caused Ca and Na leaching. Sample 13e is the kyanite-bearing mylonite

deformed sample 13c. More generally, series 13 underlines that increasing strain (from protholith to sample 13e) is first marked by leaching of Ca, Sr and Na (disappearance of plagioclase) and that this can be followed by further leaching of other elements (Mg and K), leading to passive concentration in Al and stability of kyanite.

Silica lies close to the isocon for many shear zones (Fig. 12a–d, f, g). Si seems leached in sample YCS 1b, together with Al. These elements however lie close to the line of constant volume (slope = 1), which might suggest constant volume transformation. Such a hypothesis would imply that Si, Al, and to a lesser extent Ca (also close to the constant volume line, Fig. 12e), remained the only immobile major elements during metasomatism. This seems rather unlikely especially because most shear zones are marked by the disappearance of plagioclase and an important Ca leaching (Figs. 12a, b, f–h). Consistently, although apatite crystallisation observed in sample 1b could account for some trapping of Ca, this sample shows a nearly complete disappearance of plagioclase. Constant volume deformation would also

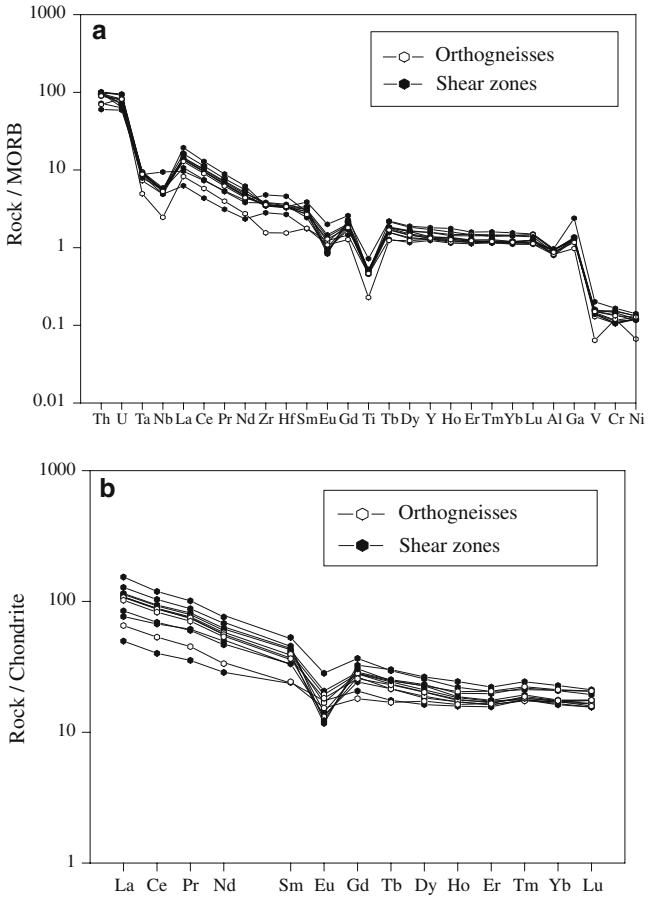

Fig. 10 Multi-element diagrams of studied samples. **a** Diagram normalized with respect to MORB (Pearce and Parkinson 1993). **b** Chondrite-normalized patterns (Taylor and Gorton 1977). Both diagrams underline the genetic similarity between orthogneisses and mylonites

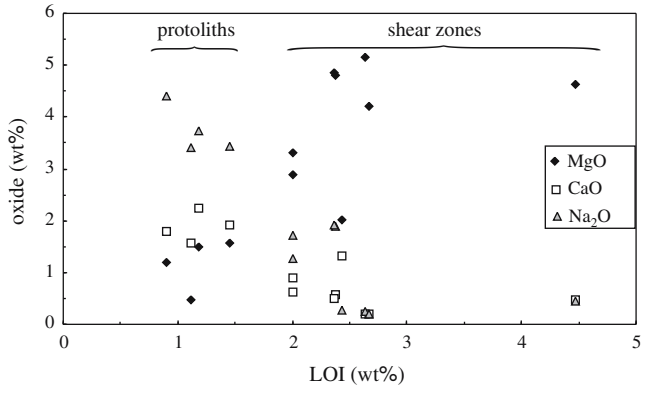

Fig. 11 Variations in oxide contents (MgO, CaO, Na_2O) according to loss on ignition (*LOI*). Increase in *LOI* is accompanied by decrease in CaO and Na_2O contents and increase in MgO content

imply a quantitative input (without fractionation) of the elements we used to define the isocon; whereas significant fractionations are observed for other elements like Nb/Ta and Th/U. Although such peculiar situation cannot be ruled out, it seems rather unlikely and would imply complex mechanisms of speciation in the fluid phase. For the above reasons, we infer that Al and Si leaching occurred in sample YCS 1b.

In contrast, silica is gained in sample YCS 7c that has an isocon slope of 0.83. All other sample pairs show isocon slopes close to one, which points to bulk constant volume transformations.

According to rock densities (Table 2), the range in isocon slopes reflects local volume losses (up to 30%, sample YCS 1b, Fig. 12e) or gains (up to 20%, sample YCS 7c, Fig. 12h), or no volume change.

Stable isotopes

Whole-rock and mineral oxygen isotope compositions are reported in Table 3 and summarized in Fig. 13. O_2 was removed from materials by reaction with BrF_5 in Ni tubes for one night at 670°C (after the method of Clayton and Mayeda 1963). It was then converted to CO_2 by reaction with hot graphite. O isotope compositions have been measured on a VG SIRA 10 mass spectrometer. Long-term analysis of NBS 28 standard ($\delta^{18}O = 9.6‰$) gave a mean value of $9.3 \pm 0.1‰$. Measured values have thus been corrected by $+0.3‰$. The analytical precision including internal errors and standard correction is estimated at $\pm 0.2‰$.

O isotope compositions of orthogneisses are consistent with the calc-alkaline nature of their protolith ($\delta^{18}O$ between 8.8 and 10.6‰). Sheared samples have $\delta^{18}O$ between 8.5 and 10.7‰. Quartz from both orthogneisses and shear zones has nearly constant $\delta^{18}O$ values (between 9.7 and 10.1‰), biotite showing more variable compositions ($\delta^{18}O$ between 4.8 and 6.3‰).

$\Delta\ ^{18}O_{Qtz\text{-}Bt}$ range between 3.7 and 4.9‰, which corresponds to high temperature isotopic equilibrium (between 470 and 605°C according to the calibration of Zheng 1993). No significant retrograde evolution is recorded by the O isotope compositions, which is consistent with microstructures and mineralogy. Orthogneisses and sheared samples have similar WR and mineral O isotope composition, which implies either that the fluid isotopic composition was buffered by host-rocks, or that infiltrating fluid and host-rock had initially similar O isotope compositions.

Discussion

Regional kinematics

Diot et al. (2002) have shown that most prominent deformation features of the Ile d'Yeu were associated with top-to-the-South thrusting. Similar kinematics un-

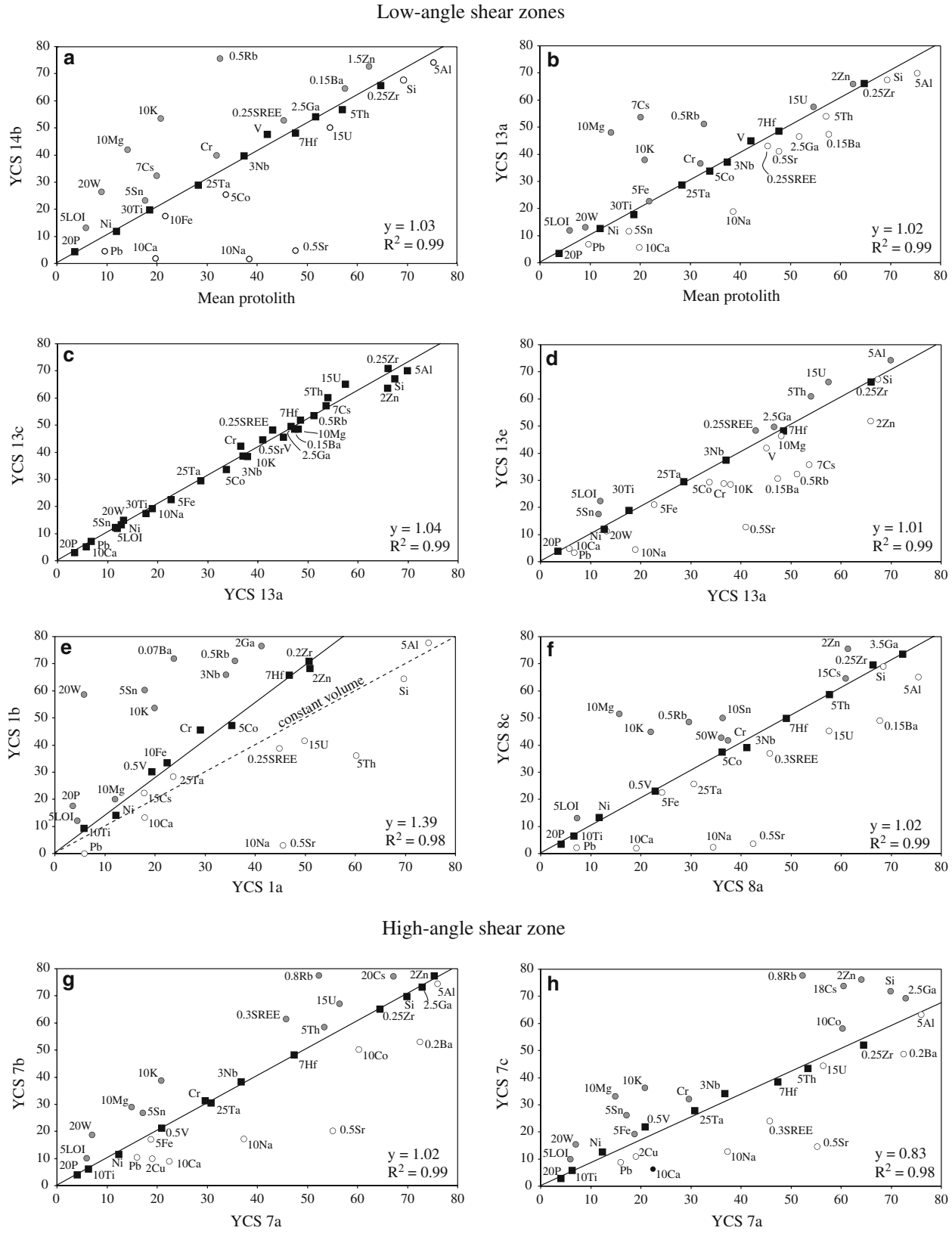

Fig. 12 Grant's (1986) diagrams showing variations in element concentration between protoliths and shear zones. Major elements are plotted as wt% oxide and trace elements as ppm (Table 3). Scaling factors are indicated. Straight lines are isocons fitted on immobile elements (*black squares*). Slope (s) and correlation coefficient (R^2) of isocons are indicated in the lower right corner of each diagram. *Grey* and *empty circles* are gained and leached elements, respectively

Table 2 Whole-rock chemical compositions and density variations across shear zones. Chemical compositions have been obtained by ICP-AES (major elements) and ICP-MS (minor elements) (SARM laboratory, CRPG-CNRS, Nancy, France) (Analytical details are available at http://www.crpg.cnrs-nancy.fr/SARM/index.html). Densities were measured on powders by He-picnometry (Orléans University)

Sample	YCS 1a	YCS 1b	YCS 7a	YCS 7b	YCS 7c	YCS 8a	YCS 8c	YCS 13a	YCS 13c	YCS 13e	YCS 14a	YCS 14b
Type	Orthogneiss	Shear zone	Orthogneiss	Shear zone	Shear zone	Orthogneiss	Shear zone	Orthogneiss	Shear zone	Shear zone	Orthogneiss	Shear zone
SiO_2	69.67	64.49	69.89	69.74	71.94	68.42	69.01	67.35	67.05	67.21	76.49	67.70
Al_2O_3	14.93	15.52	15.19	14.90	12.70	15.09	13.03	13.98	14.01	14.89	13.13	14.84
Fe_2O_3	4.48	6.68	3.75	3.42	3.85	4.85	4.51	4.53	4.51	4.22	1.77	3.51
MnO	< dl	0.03	0.03	0.03	0.03	0.05	< dl	< dl	< dl	< dl	< dl	0.03
MgO	1.20	2.01	1.49	2.90	3.32	1.57	5.15	4.81	4.86	4.64	0.47	4.21
CaO	1.79	1.32	2.24	0.90	0.63	1.91	0.20	0.57	0.51	0.48	1.56	0.19
Na_2O	4.40	0.27	3.73	1.72	1.28	3.44	0.24	1.89	1.92	0.44	3.41	0.19
K_2O	1.99	5.37	2.08	3.87	3.63	2.20	4.49	3.79	3.85	2.85	1.93	5.34
TiO_2	0.58	0.92	0.63	0.62	0.58	0.66	0.65	0.59	0.58	0.63	0.29	0.66
P_2O_5	0.18	0.88	0.20	0.20	0.14	0.20	0.17	0.17	0.15	0.19	0.07	0.21
LOI	0.90	2.43	1.18	2.01	2.00	1.45	2.63	2.38	2.37	4.47	1.12	2.67
Total	100.1	99.9	100.4	100.3	100.1	99.8	100	100.1	99.8	100	100.2	99.6
La	34.20	24.16	34.06	48.46	15.67	33.80	26.67	32.17	35.65	36.26	20.59	40.33
Ce	71.76	54.76	72.01	96.87	32.60	70.92	56.28	67.29	75.14	76.40	43.34	84.30
Pr	8.58	7.12	8.84	11.72	4.12	8.69	6.97	8.20	9.19	9.47	5.24	10.22
Nd	33.53	29.68	34.42	45.35	17.11	33.34	27.87	32.04	35.88	37.29	19.97	40.56
Sm	7.19	7.62	7.71	10.18	4.61	7.57	6.41	7.02	8.11	8.20	4.67	8.77
Eu	0.95	0.85	1.40	2.04	1.26	1.21	0.97	1.31	1.49	1.03	1.11	0.89
Gd	6.84	8.42	7.23	9.50	5.36	7.33	6.29	6.65	7.45	7.27	4.68	7.92
Tb	1.05	1.48	1.15	1.45	0.86	1.21	1.05	1.13	1.24	1.19	0.83	1.21
Dy	6.12	8.62	6.62	8.32	5.29	7.36	5.94	6.58	7.52	6.85	5.61	7.36
Ho	1.24	1.78	1.30	1.61	1.16	1.49	1.25	1.28	1.45	1.34	1.19	1.36
Er	3.48	4.72	3.58	4.37	3.33	4.39	3.45	3.65	4.20	3.68	3.53	3.74
Tm	0.52	0.73	0.55	0.64	0.53	0.67	0.53	0.55	0.65	0.53	0.56	0.58
Yb	3.54	4.73	3.61	4.35	3.53	4.40	3.38	3.58	4.32	3.44	3.63	3.67
Lu	0.53	0.68	0.54	0.66	0.57	0.67	0.50	0.51	0.63	0.50	0.57	0.57
Ba	340	1028	362	265	244	451	327	316	324	204	347	430
Pb	5.94	< dl	15.95	10.4	8.80	7.13	2.20	6.76	7.06	3.36	19.3	4.47
Sr	91.1	6.10	110	40.5	29.3	84.9	7.19	82.0	89.1	25.6	99.5	9.28
Rb	71.9	142	65.4	96.8	97.0	59.3	97.2	102	107	64.7	46.4	151
Cs	1.19	1.49	3.36	3.86	4.12	4.06	4.31	7.67	8.15	5.10	2.90	4.63
U	3.32	2.77	3.76	4.47	2.96	3.84	3.01	3.84	4.34	4.42	3.88	3.34
Th	12.0	7.22	10.7	11.7	8.68	11.5	11.7	10.8	12.0	12.2	8.36	11.4
Ta	0.95	1.14	1.23	1.22	1.11	1.23	1.03	1.15	1.18	1.18	0.64	1.16
Nb	11.4	22.0	12.3	12.8	11.4	13.7	13.0	12.3	12.9	12.5	5.73	13.3
Zr	254	354	258	260	208	265	278	264	284	265	115	262
Hf	6.68	9.40	6.77	6.89	5.50	7.01	7.12	6.94	7.40	6.87	3.17	6.87
Y	36.0	50.7	37.4	48.0	34.6	44.2	35.9	37.1	43.7	38.4	35.9	38.6
Zn	25.5	34.1	37.7	38.7	44.8	30.7	37.7	33.0	31.8	26.0	35.4	48.6
Ga	20.6	38.2	20.8	20.9	19.8	20.7	21.0	18.7	19.8	19.9	15.6	21.7
Ni	12.2	14.1	12.3	11.7	12.7	11.6	13.2	12.8	13.2	11.9	6.68	12.0
Cr	29.0	45.5	29.6	31.3	32.1	37.4	41.8	36.6	42.3	28.8	32.9	40.1
Co	7.07	9.45	6.03	5.03	5.82	7.25	7.48	6.75	6.74	5.87	3.92	5.09
Cu	< dl	< dl	9.50	4.95	5.44	13.45	< dl	< dl	< dl	< dl	18.62	< dl
V	38.8	60.4	41.8	42.3	43.7	45.7	45.9	45.1	45.6	42.0	19.3	47.5
Mo	< dl	< dl	0.47	< dl	< dl	1.54	< dl	0.46	< dl	0.46	0.87	0.56
Sn	3.58	12.1	3.42	5.36	5.22	3.63	5.01	2.31	2.46	3.50	1.73	4.67
W	0.29	2.93	0.35	0.94	0.77	0.72	0.85	0.66	0.74	0.56	0.44	1.33
Density	2.710	2.801	2.715	2.739	2.735	2.729	2.769	2.739	2.736	2.714		

der similar metamorphic conditions is consistently observed in the Sables d'Olonne area (Fig. 1) (Iglesias and Brun 1976; Brun and Burg 1982; Cannat and Bouchez 1986). If overall southward to SSE thrust motions are well established, they do not straightaway account for the scatter in stretching lineation observed within shear zones (Fig. 4b) and to a lesser extent within the orthogneiss itself (Fig. 4a). Such scatter in stretching lineations implies finite flattening strains (see Gapais et al. 1987), a feature that cannot be excluded in an overall thrusting context. However, the structural and metamorphic pattern observed on the Ile d'Yeu appears quite similar to that from the Sables d'Olonne area (Fig. 1), where combinations of N–S and E–W stretching have been shown to result from syn-convergence E–W extension overprinting top-to-the-South thrusting (Cagnard et al. 2004). In this area, the overprint is nearly complete within metapelitic units, but NS stretching

Table 3 Oxygen isotope data (‰) across the five studied shear zones. Qtz-Bt equilibrium temperatures according to Zheng (1993)

Sample	Type	$\delta^{18}O_{WR}$	$\delta^{18}O_{Qtz}$	$\delta^{18}O_{Bt}$	$\Delta_{Qtz\text{-}Bt}$	$T(°C)_{Qtz\text{-}Bt}$
YCS 1a	Orthogneiss	8.8	9.7	4.8	4.9	470 ± 40
YCS 1b	Shear zone	8.5	9.8	5.4	4.3	520 ± 40
YCS 7a	Orthogneiss	10				
YCS 7b	Shear zone	9.7				
YCS 7c	Shear zone	10				
YCS 8a	Orthogneiss	9.7	10.1	5.7	4.4	520 ± 40
YCS 8c	Shear zone	8.9	9.7	6	3.7	605 ± 60
YCS 13a	Orthogneiss	9.4	10.1	6.3	3.8	590 ± 60
YCS 13c	Shear zone	9.4				
YCS 13e	Shear zone	10.7				
YCS 14a	Orthogneiss	10.6				
YCS 14b	Shear zone	9.8				

lineations associated with top-to-the-South thrusting are well preserved within quartzites and in a pre-tectonic orthogneiss similar to that of the Ile d'Yeu. This was probably due to strong ductility contrasts between dry and water-rich units under HT partial melting conditions (Cagnard et al. 2004). As in the Sables d'Olonne area, individual shear zones from the Ile d'Yeu orthogneiss show local changes in the direction of the stretching lineation on individual foliation planes, a feature best explained by combinations of superposed kinematics (Brun and Burg 1982).

From the comparison between the Ile d'Yeu and the Sables d'Olonne area, we thus propose that the observed deformation pattern results from N–S to NNW thrusting motion partially overprinted by E–W extensional deformations that allowed the exhumation of this lower crustal level. Extension may, in particular, be responsible for the late E–W to NW–SE boudinage observed on the island (Fig. 5d). Extension and associated exhumation of HT rocks in South Brittany is of Upper Carboniferous age, around 310–300 Ma (Gapais et al. 1993; Colchen and Rolin 2001; Cagnard et al. 2004). Consistently, recent Ar-Ar analyses obtained on white micas from the Ile d'Yeu have yielded cooling ages of about 300 Ma (Diot, unpublished data).

Timing of strain localization

The Ile d'Yeu orthogneiss is marked by both strong strain localization within outcrop-scale shear zones and distributed deformations recorded by the regional foliation and lineation. Deformation patterns, microstructures and mineralogy show that both types of structures have recorded HT conditions. Deformations during subsequent cooling have been rather limited, as underlined by the lack of significant syn-kinematic growth of low-grade minerals and by the static aspect of kyanite-to-cordierite retrogression (Fig. 7e) (Semelin and Marchand 1984).

Fluid-assisted growth of phyllosilicates at the expense of feldspars, as observed within the Ile d'Yeu shear zones, is a particularly efficient softening mechanism (e.g. Mitra 1978; White and Knipe 1978; Marquer et al. 1985; Fitzgerald and Stünitz 1993; Wibberley 1999; Bos et al. 2000; Gueydan et al. 2003). In the Ile d'Yeu orthogneiss, metasomatic transformations are only observed within shear zones. In addition, a good geometrical consistency is observed between shear zone pattern and regional pervasive fabrics (Fig. 4). These features underline that metasomatic transformations occurred during shear zone development and favoured shear localization, but did not predate it. On the other hand, it is unlikely that the onset of shear localization occurred around the thermal peak. Indeed, limited strain localization is expected during amphibolite facies deformation of granitic rocks because feldspars are ductile, may recrystallise and show low strength contrasts with quartz (see Gapais 1989). Best potential candidates for the timing of shear zone initiation are therefore either the prograde history or the retrograde one. Arguments that fit with an onset of the localization process during the prograde path are :

- The lack of syn-kinematic growth of chlorite after biotite within shear zones shows that fluid-assisted deformation ceased relatively early during the retrograde path.
- Isotopic equilibrium temperatures between quartz and biotite are estimated around 500–600°C (Table 3) and correspond to the closing of oxygen isotopic exchange between syn-kinematic minerals and fluids. This imposes that no active fluid circulation occurred below 500–600°C along the retrograde path.
- As the growth of syn-kinematic micas and kyanite results from channelled mass transfer and passive concentration of Al, it must follow or at least be coeval with shear localization. Semelin and Marchand (1984) have argued that kyanite-bearing assemblages developed somewhere around the pressure peak, and were followed by local partial melting and then by growth of retrogressive minerals.
- Most shear zones lie at very low angle to the regional foliation and show evidence of parallel stretch. They thus underwent significant strains, which supports relatively early localization during progressive deformation. In general, a syn-tectonic prograde path should be accompanied by shear localization because

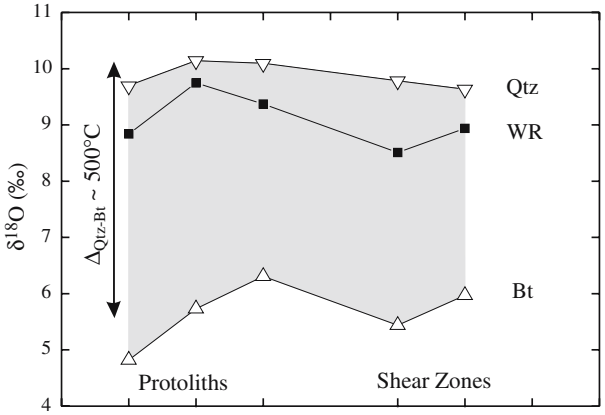

Fig. 13 Synthetic diagram showing O isotope data (‰) from whole rock (*WR*), biotite (*Bt*) and quartz (*Qtz*) within selected protoliths and shear zones. Qtz-Bt fractionation at 500°C is from Zheng (1993)

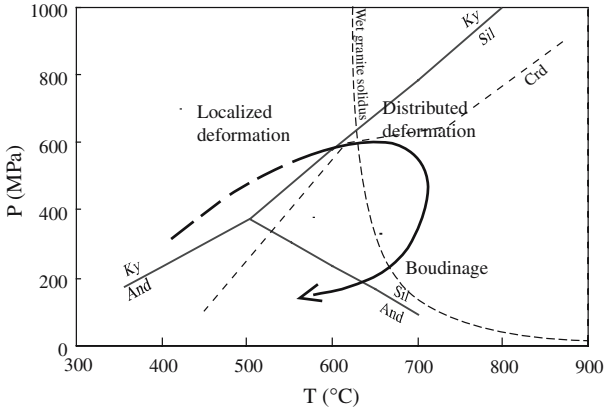

Fig. 14 Main steps of structural evolution of the Ile d'Yeu orthogneiss and associated shear zones during burial and exhumation. PT path is modified after Semelin and Marchand (1984). Water-saturated granite solidus line is from Holtz et al. (2001). Al-silica triple junction is from Holdaway (1971). The cordierite field is from Spear (1993). See text for further comments

(1) deformation at moderate temperatures favours grain size reduction and subsequent strain and (or) reaction softening, (2) primary magmatic heterogeneities, like local concentrations in phyllosilicates, may favour shear zone nucleation, and (3) reactivation of structures like faults or joints may trigger early fluid channelling and associated reaction softening and shear localization (e.g. Mancktelow and Pennacchioni 2005). Field evidence further shows that outcrops where shear zones are abundant also present significant volumes of rather weakly deformed orthogneiss; whereas shear zone-free outcrops generally show a more homogeneous penetrative fabric. This is consistent with rather early localization allowing local preservation of weakly deformed domains. More generally, stretching of shear zone arrays in the course of a continuous progressive deformation requires that strains accumulate within neighbouring domains. The regional orthogneissic fabric must therefore have in part developed after localization, during rotation and stretching of the shear zones. From the above arguments, we propose that progressive deformation involved strain localization along shear zones somewhere along the prograde metamorphic path. Increase in temperature around pressure peak conditions or during early decompression (Fig. 14; Semelin and Marchand 1984) was then accompanied by an increase in distributed deformation with respect to shear zone development, leading to stretching of early shear zones. The high-angle shear zone (series 7) does not show evidence of late stretching, is marked by a rather progressive strain gradient (Fig. 6b), and appears as a ramp between two flat-lying zones (Fig. 5c). These features suggest that this zone might have formed relatively late during the building of the shear zone array. The filling of boudin necks by shear zone products, as well as the growth of late cordierite, marks the decay of shear zone activity (Fig. 14).

A model of fluid-assisted progressive deformation

The geochemical analysis shows that the studied mylonites, especially the kyanite-bearing one (sample YCS 13e), resulted from extreme metasomatism. Comparable examples, marked by the growth of sillimanite, have been described in the literature (Vernon 1979; Musumeci 2002). These authors proposed that the growth of Al-silicates was due to base-cation leaching of pre-existing silicates, either by hydrogen metasomatism (Vernon 1979), or by replacement of K-feldspar or biotite and albite-rich plagioclase due to pressure solution assisted by circulation of acidic fluids not buffered by the rock composition (Musumeci 2002). In the present example, there is no evidence that kyanite replaces older phases. Its growth may simply be due to the leaching of Ca, Na and, to a lesser extend K, inducing an important excess of Al within the mylonite YCS 13e.

The major metasomatism documented in the shear zones implies large time-integrated fluid fluxes (Dipple and Ferry 1992). For example, Selverstone et al. (1991) have calculated values close to 8×10^6 m^3/m^{-2} in a Si-depleted shear zone with up to 60% volume loss, and Cartwright and Buick (1999) obtained values between 5.9×10^4 and 4.2×10^5 m^3/m^{-2} in a Si-enriched zone with 11% volume increase. In the present example, the source of important amounts of fluids may be found within underthrust metapelites that underwent dehydration metamorphic reactions during burial.

O isotope data are consistent with fluids coming from deep metasedimentary rocks. The flow of low $\delta^{18}O$ surface-derived fluids cannot be invoked because it would have lowered the O isotope composition of infiltrated rocks, as for example documented by Cartwright and Buick (1999). Such a decrease in $\delta^{18}O$ values is not observed within the studied shear zones (Fig. 13, Table 3). On the other hand, high Qtz-Bt apparent equilibration temperatures (Table 3) are not incompatible

with an initiation of fluid flow at low or moderate temperatures. Indeed, an increase in temperature leads to a continuous isotopic re-equilibration between minerals. Then, re-equilibration stops on the retrograde path as temperature further decreases. Therefore, isotopic temperature estimates refer to latest re-equilibration stages along the retrograde path. For the high temperature fluid flow event, H_2O in equilibrium with quartz of shear zones ($\delta^{18}O = 9.7‰$) at 600°C would have a $\delta^{18}O$ value of *ca.* 7.6‰ (Zheng 1993). This value is within the range of metamorphic fluids (Sheppard 1986). Quartz grains from orthogneisses and shear zones have nearly identical $\delta^{18}O$ values that could correspond to an unmodified primary O isotope composition (Table 3, Fig. 13). This probably shows that fluids experienced isotopic exchange with the orthogneiss during their upward circulation.

Figure 15 shows the general frame of successive stages that may occur in a collisional context marked by thickening and subsequent extensional uplift, as can be inferred for the Ile d'Yeu area. In an overall thrusting context, where initially rather cold sediments are buried under hotter units, one can expect upward fluid motions on a wide temperature range because of the numerous dehydration metamorphic reactions encountered as temperature increases in the footwall. One can further expect that thermal re-equilibration might induce changes from up-temperature to subsequent down-temperature fluid flow coming from the footwall (Fig. 15a, b). Selverstone et al. (1991) have for example documented early up-temperature upward fluid flow within amphibolite-grade shear zones (Tauern Window gneisses, Eastern Alps) that resulted in a drastic loss of silica and an associated huge volume decrease (about 60 %). On the other hand, Cartwright and Buick (1999) described mid-crustal shear zones marked by significant volume increase (up to 11%) associated with gains in Si and K, and depletion in Na and Ca, and due to down-temperature flow. This behaviour is consistent with that proposed by Dipple and Ferry (1992) who further showed that the solubility of Na and Ca within HT aqueous fluids varied similarly along a temperature gradient, Si and K varying in the opposite direction. In the shear zone array of the Ile d'Yeu, that may have evolved over a rather long portion of the PT path, one should expect that early initiated shear zones record the effects of infiltration over a wide temperature range compared with latest ones.

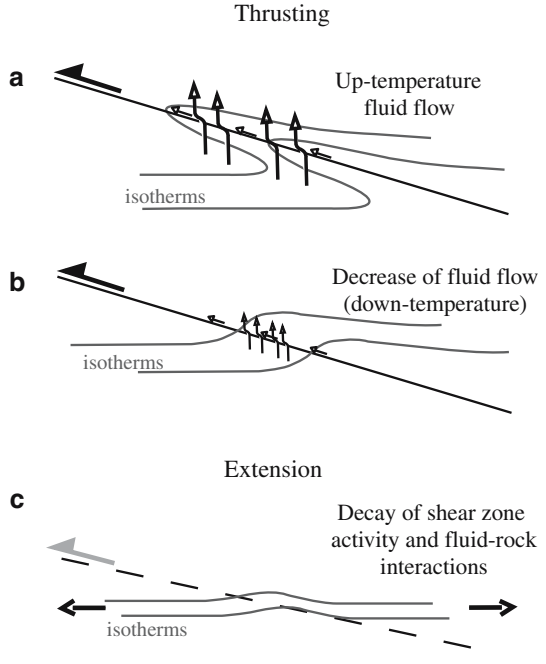

Fig. 15 Not to scale. Cartoons summarizing the theoretical evolution of thermal conditions and associated fluid flows in an orogenic belt, from early thrusting (**a**) to extensional exhumation (**c**)

The high-angle shear zone (series 7) that probably formed relatively late in the history is marked by a Si gain and a volume increase of about 20% (Fig. 12h). It might thus have recorded down-temperature fluid flow during high-temperature shearing. This shear zone is also enriched in W and Sn (Fig. 12h), a feature often associated with circulation of high-temperature fluids during the emplacement of granitic magmas (forming skarns for example, see review of Newberry 1998). The enrichment in W and Sn might thus be associated with flow of fluids generated from high-temperature reactions, including partial melting of underlying metasedimentary rocks. Consistently, Semelin and Marchand (1984) have reported partial melting within the Ile d'Yeu paragneisses (see PT path, Fig. 14).

Many low-angle shear zones, except series 13, are also significantly enriched in W and Sn, and were thus the locus of high-temperature fluid circulation. None of them however displays significant volume loss and Si gain, as expected for such circulation situation. With respect to the other shear zones, series 1 displays an extreme behaviour, with a volume decrease of about 30% and Si and Al losses (Fig. 12e). Si loss in this shear zone might reflect down-temperature fluid flow, as expected to occur during early stages of thrusting, the combined peculiar behaviour of Al remaining a question that would require further study. Thus, a possible interpretation of the irregular volume changes in low-angle shear zones and erratic behaviours of some chemical species might reflect variable records of successive up-temperature (volume and Si losses) and down-temperature (volume and Si gains, W and Sn enrichment) fluid channelling, according to the timing of shear zone development and to their local individual evolution.

Conclusions

Both metamorphic and structural features recorded on the Ile d'Yeu are consistent with those established in the Sables d'Olonne area, where the equivalent of the Ile d'Yeu orthogneiss (Mathieu 1945) is observed in the deepest parts of the tectonic pile. Structures are consis-

tent with top-to-the-South thrusting (Diot et al. 2002) partially overprinted by E–W syn-convergence extension associated with exhumation.

The prograde history of the Ile d'Yeu orthogneiss was marked by sharp strain localization along shear zones. During shearing, extensive fluid channelling led to a change from a Qtz + Pl + Kfs + Bt ± Ms mineralogy to more aluminous micaschist assemblages made of Bt + Ms + Qtz ± Ky. Mass transfers record gains in H_2O, K, Mg, P, Rb, W, Sn, and losses in Ca, Na, Sr and Pb.

Volume changes across the shear zones studied are generally minor, but may have recorded either gains (+20%) or losses (−30%). This apparent inconsistency might be related to early upward channelling of fluids during crustal thickening and associated thermal re-equilibration, with early up-temperature fluid flow followed by variable amounts of overprints by down-temperature fluid flow.

Oxygen isotopes indicate that fluid-rock interactions within shear zones stopped during early stages of exhumation and cooling, at temperatures around 500–600°C, a feature supported by HT syn-kinematic microstructures and by the limited growth of late-kinematic retrograde minerals. Distributed deformations followed the development of most shear zones. Associated stretching, with boudin necks filled by stretched shear zone mylonites, marks the decay of shear zone activity.

Acknowledgements This work was the MsC research project of C.S., made in the frame of the ARMOR 2 program (Géofrance 3D, BRGM-CNRS). E. Bénéteau and the Laboratoire d'Etude des Bio-Indicateurs Marins are thanked for their hospitality and field assistance on the Ile d'Yeu. J. Cornichet helped during analytical sessions. The paper benefited from constructive discussions with M. Ballèvre, J.P. Brun, and P. Pitra. We are indebted to A-M. Boullier and D. Marquer for very constructive reviews that greatly improved the early version of the paper.

References

Ashworth JR (1986) Myrmekite replacing albite in prograde metamorphism. Am Mineral 71:895–899

Beach A (1976) The interrelations of fluid transport, deformation, geochemistry and heat flow in early Proterozoic shear zones in the Lewisian complex. Philos Trans R Soc Lond 280:569–604

Blenkinsop T (2000) Deformation microstructures and mechanisms in minerals and rocks. Kluwer, Dordrecht, pp 1–150

Bos B, Peach CJ, Spiers CJ (2000) Frictional-viscous flow of simulated fault gouge caused by the combined effects of phyllosilicates and pressure solution. Tectonophysics 327:173–194

Bosse V, Ballèvre M, Vidal O (2002) Ductile thrusting recorded by the garnet isograde from the blueschist-facies metapelites of the Ile de Groix, Armorican Massif, France. J Petrol 43:485–510

Brown MD, Dallmeyer RD (1996) Rapid Variscan exhumation and the role of magma in core complex formation: southern Brittany metamorphic belt, France. J Metamorphic Geol 14:361–379

Brun JP, Burg JP (1982) Combined thrusting and wrenching in the Ibero-Armorican arc: a corner effect during continental collision. Earth Planet Sci Lett 61:319–332

Burg JP, Van Den Driessche J, Brun JP (1994) Syn-to post thickening in the Variscan Belt of the Western Europe: modes and structural consequences. Géologie de la France 3:33–51

Cagnard F, Gapais D, Brun JP, Gumiaux C, Van Den Driessche J (2004) Late Hercynian crustal-scale extension in Vendée (Armorican Massif, France). J Struct Geol 26(3):435–449

Cannat M, Bouchez JL (1986) Linéations N-S et E-W en Vendée littorale (Massif Armoricain). Episodes tangentiels successifs à foliation horizontale. Soc Géol France Bull 16: 299–310

Cartwright I, Buick IS (1999) The flow of surface-derived fluids through Alice Springs age middle-crustal ductile shear zones, Reynolds Range, Central Australia. J Metamorphic Geol 17:397–414

Clayton RN, Mayeda TK (1963) The use of bromine pentafluoride in the extraction of oxygen from oxides and silicates for isotopic analysis. Geochim Cosmochim Acta 27(1):43–52

Colchen M, Rolin P (2001) La chaîne hercynienne en Vendée. Géologie de la France 1–2:53–85

Diot H, Gauffriau A, Femenias O, Mercier J, Mauroy M (2002) L'île d'Yeu : mémoire des évènements éodévoniens en bordure Sud de l'Armorique. In: 19th Réunion des Sciences de la Terre Nantes, Abstr with Prog, pp 108–109

Dipple GM, Ferry JM (1992) Metasomatism and fluid flow in ductile fault zones. Contrib Mineral Petrol 112:149–164

Dipple GM, Wintsch RP, Andrews S (1990) Identification of the scales of differential element mobility in a ductile fault zone. J Metamorphic Geol 8:645–661

Etheridge MA, Wall VJ, Vernon RH (1983) The role of the fluid phase during regional metamorphism and deformation. J Metamorphic Geol 1:205–226

Etheridge MA, Wall VJ, Cox SF (1984) High fluid pressures during regional metamorphism and deformation: implications for mass transport and deformation mechanisms. J Geophys Res 89:4344–4358

Fitzgerald JD, Stünitz H (1993) Deformation of granitoïds at low metamorphic grade. I: reactions and grain size reduction. Tectonophysics 221:269–297

Gapais D (1989) Shear structures within deformed granites: mechanical and thermal indicators. Geology 17:1144–1147

Gapais D, Barbarin B (1986) Quartz fabric transition in a cooling syntectonic granite (Hermitage Massif, France). Tectonophysics 125:357–370

Gapais D, Balé P, Choukroune P, Cobbold PR, Majhoub Y, Marquer D (1987) Bulk kinematics from shear zone patterns: some field examples. J Struct Geol 9:635–646

Gapais D, Lagarde JL, Le Corre C, Audren C, Jégouzo P, Casas Sainz A, Van Den Driessche J (1993) La zone de cisaillement de Quiberon : témoin d'extension de la chaîne varisque en Bretagne méridionale au Carbonifère. C R Acad Sci Paris Sér II 316:1123–1129

Goujou JC (1992) Analyse pétro-structurale dans un avant-pays métamorphique: influence du plutonisme tardi-orogénique varisque sur l'encaissant épi à méso zonal de Vendée. Doc Bur Rech Géol Min 216

Grant JA (1986) The Isocon diagram—a simple solution to Gresens' equation for metasomatic alteration. Econ Geol 81:1976–1982

Gueydan F, Leroy YM, Jolivet L, Agard P (2003) Analysis of continental midcrustal strain localization induced by reaction-softening and microfracturing. J Geophys Res 108(B2), 2064. DOI:10.1029/2001JB000611

Holdaway MJ (1971) Stability of andalusite and the aluminum silicate phase diagram. Am J Sci 271:97–131

Holtz F, Johannes W, Tamic N, Behrens H (2001) Maximum and minimum water contents of granitic melts generated in the crust: a reevaluation and implications. Lithos 56:1–14

Hughes CJ (1973) Spilites, keratophyres, and the igneous spectrum. Geol Mag 109:513–527

Iglesias M, Brun JP (1976) Signification des variations et anomalies de la déformation dans un segment de la chaîne hercynienne (les séries crystallophylliennes de la Vendée littorale, Massif Armoricain). Soc Géol France Bull 7:1443–1452

Jégouzo P (1980) The South Armorican shear zone. J Struct Geol 2:39–47

Jones KA, Brown M (1990) High-temperature "clockwise" P-T paths and melting in the development of regional migmatites: an example from Southern Brittany, France. J Metamorphic Geol 14:361–379

Kerrich R (1986) Fluid infiltration into fault zones: chemical, isotopic and mechanical effects. Pure Appl Geophys 124:225–268

Le Hébel F, Vidal O, Kienast JR, Gapais D (2002) Evidence for HP-LT Hercynian metamorphism within the "porphyroïds" of South Brittany. C R Geosci 334:205–211

Mainprice D, Bouchez JL, Blumenfeld P, Tubia JM (1986) Dominant c-slip in naturally deformed quartz: implications for dramatic plastic softening at high temperature. Geology 14:819–822

Mancktelow NS, Pennacchioni G (2005) The control of precursor brittle fracture and fluid-rock interaction on the development of single and paired ductile shear zones. J Struct Geol 27: 645–661

Maniar PD, Piccoli PM (1989) Tectonic discrimination of granitoids. Geol Soc Am Bull 101:635–643

Marquer D, Burkhard M (1992) Fluid circulation, progressive deformation and mass-transfer processes in the upper crust: the example of basement-cover relationships in the External Crystalline Massifs, Switzerland. J Struct Geol 14:1047–1057

Marquer D, Gapais D, Capdevila R (1985) Chemical changes and mylonitisation of a granodiorite within low-grade metamorphism (Aar Massif, Central Alps). Bull Mineral 108:209–221

Mathieu G (1945) La Géologie de l'Ile d'Yeu. Carte Géol France Bull 219:479–518

McCaig AM (1988) Deep fluid circulation in fault zones. Geology 16:867–870

Mitra G (1978) Ductile deformation zones and mylonites: the mechanical process involved in the deformation of crystalline basement rocks. Am J Sci 278:1057–1084

Musumeci G (2002) Sillimanite-bearing shear zones in syntectonic leucogranite: fluid-assisted brittle-ductile deformation under amphibolite facies conditions. J Struct Geol 24:1491–1505

Newberry RJ (1998) W- and Sn-skarn deposits: a 1998 status report. In: Lentz DR (ed) Mineralized intrusion-related skarn systems. Min Assoc Can Short Course Series vol 26:289–335

Newton RC (1990) Fluids and shear zones in the deep crust. Tectonophysics 182:21–37

Pearce JA, Parkinson IJ (1993) Trace element models for mantle melting: application to volcanic arc petrogenesis. In: Prichard HM, Alabaster T, Harris NBW, Neary CR (eds) Magmatic processes and plate tectonics. Geol Soc London Spec Pub 76:373–403

Rolland Y, Cox S, Boullier AM, Pennacchioni G, Mancktelow N (2003) Rare earth and trace element mobility in mid-crustal shear zones: insights from the Mont Blanc Massif (Western Alps). Earth Planet Sci Lett 214: 203–219

Selverstone J, Morteani G, Staude JM (1991) Fluid channelling during ductile shearing: transformation of granodiorite into aluminous schist in the Tauern Window, Eastern Alps. J Metamorphic Geol 9:419–431

Semelin B, Marchand J (1984) Découvertes d'enclaves hyper-alumineuses dans l'orthogneiss de l'Ile d'Yeu. C R Acad Sci Paris Série II 299(10):633–638

Sheppard SMF (1986) Stable isotope variations in natural waters. In: Valley JW, Taylor HP, O'Neil JR (eds) Stable isotopes in high temperature geologic processes. Rev Mineral Geochem 16:319–372

Simpson C (1985) Deformation of granitic rocks across the brittle-ductile transition. J Struct Geol 7(5):503–511

Spear FS (1993) Metamorphic phase equilibria and pressure-temperature-time paths. Min Soc Am Monograph, 799pp

Taylor SR, Gorton MP (1977) Geochemical application of spark source mass spectrography—III. Element sensitivity, precision and accuracy. Geochim Cosmochim Acta 41:1375–1380

Triboulet C, Audren C (1988) Controls of P-T-t deformation path from amphibole zonation during progressive metamorphism of basic rocks (estuary of the River Vilaine, South Brittany, France). J Metamorphic Geol 6:117–133

Vernon RH (1979) Formation of late sillimanite by hydrogen metasomatism (base-leaching) in some high-grade gneisses. Lithos 12:143–152

Voll G (1976) Recrystallisation of quartz, biotite and felsdpars from Erst feld to the Leventina Nappe, Swiss Alps, and its geological significance. Schweitz Mineral Petrogr Mitt 56:641–647

White SH, Knipe RJ (1978) Transformation- and reaction-enhanced ductility in rocks. J Geol Soc London 135:513–516

Wibberley C (1999) Are feldspar-to-mica reactions necessarily reaction-softening process in fault zones. J Struct Geol 21:1219–1227

Wyns R, Calvez JY, Chantraine J, Peucat JJ (1986) Mise en évidence d'un socle précambrien en Vendée-Maritime. Géodynamique du Massif Armoricain RCP 705

Yonkee WA, Parry WT, Bruhn RL (2003) Relations between progressive deformation and fluid-rock interaction during shear-zone growth in a basement-cored thrust sheet, sevier orogenic belt, Utah. Am J Sci 303:1–59

Zheng YF (1993) Calculation of oxygen isotope fractionation in anhydrous silicate minerals. Geochim Cosmochim Acta 57:1079–1091